LLNL-JRNL-608956

LAWRENCE
LIVERMORE
NATIONAL
LABORATORY

A New Level Set Model

D. P. Starinshak, S. Karni, P. L. Roe

December 20, 2012

Journal of Computational Physics

Disclaimer

This document was prepared as an account of work sponsored by an agency of the United States government. Neither the United States government nor Lawrence Livermore National Security, LLC, nor any of their employees makes any warranty, expressed or implied, or assumes any legal liability or responsibility for the accuracy, completeness, or usefulness of any information, apparatus, product, or process disclosed, or represents that its use would not infringe privately owned rights. Reference herein to any specific commercial product, process, or service by trade name, trademark, manufacturer, or otherwise does not necessarily constitute or imply its endorsement, recommendation, or favoring by the United States government or Lawrence Livermore National Security, LLC. The views and opinions of authors expressed herein do not necessarily state or reflect those of the United States government or Lawrence Livermore National Security, LLC, and shall not be used for advertising or product endorsement purposes.

A New Level Set Model *

David P. Starinshak, Smadar Karni, and Philip L. Roe

December 12, 2012

Abstract

We present a new level set model for representing multimaterial flows in multiple space dimensions. Instead of associating a level set function with a specific fluid material, the function is associated with a pair of materials and the interface that separates them. A voting algorithm collects sign information from all level sets and determines material designations. $M(M-1)/2$ level set functions might be needed to represent a general M-material configuration; problems of practical interest use far fewer functions, since not all pairs of materials share an interface. The new model is less prone to producing indeterminate material states, i.e. regions claimed by more than one material (overlaps) or no material at all (vacuums). It outperforms existing material-based level set models without the need for reinitialization schemes, thereby avoiding additional computational costs and preventing excessive numerical diffusion.

1 Introduction

Level sets provide a convenient model to represent multimaterial fluids and follow their dynamics. The interface between material components is embedded as the zero curve of a level set function $\phi(\mathbf{x}, t)$ with signs identifying

$$\phi(\mathbf{x}, t) \begin{cases} > 0 & , \quad (\mathbf{x}, t) \text{ in material 1} \\ < 0 & , \quad (\mathbf{x}, t) \text{ not in material 1} \end{cases} \tag{1}$$

The zero level curve $G(t) = \{\mathbf{x}(t) : \phi(\mathbf{x}, t) = 0\}$ defines the interface separating regions occupied by material 1 from regions that are not. In fluid dynamics, interfaces are often carried by the fluid flow and are governed by

$$\frac{\partial \phi}{\partial t} + \mathbf{u} \cdot \nabla \phi = 0, \tag{2}$$

where $\mathbf{u}$ denotes the underlying fluid velocity.

If the number of materials is two, one may represent the subregions occupied by the fluid components with the functions

$$\phi_1(\mathbf{x}, t) \begin{cases} > 0 & , \quad (\mathbf{x}, t) \text{ in material 1} \\ < 0 & , \quad (\mathbf{x}, t) \text{ in material 2} \end{cases} \qquad \phi_2(\mathbf{x}, t) \begin{cases} > 0 & , \quad (\mathbf{x}, t) \text{ in material 2} \\ < 0 & , \quad (\mathbf{x}, t) \text{ in material 1} \end{cases} \tag{3}$$

*This work was supported by DOE NNSA-ASC grant DE-FC52-08NA28616 and NSF Award # DMS 0609766

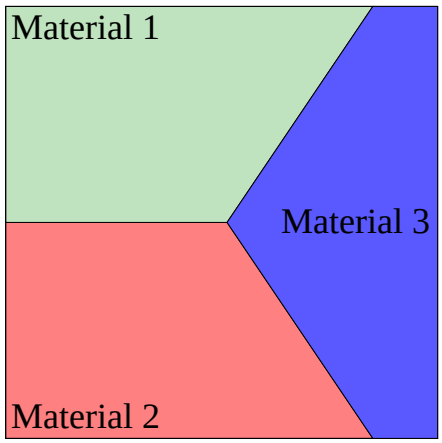

Figure 1: Intersection of three materials at a Y-shaped triple junction.

Clearly, this model is redundant: if a region is not occupied by material 1, it must be occupied by material 2. In this situation, one level set function is sufficient to partition the domain, and its zero level curve may be viewed as separating the two materials:

$$\phi_{1,2}(\mathbf{x},t) \begin{cases} > 0 & , \quad (\mathbf{x},t) \text{ in material 1} \\ < 0 & , \quad (\mathbf{x},t) \text{ in material 2} \end{cases} \tag{4}$$

From a computation viewpoint, redundancies are inefficient. But more importantly, they have the potential of creating computational inconsistencies. For instance, using (3), the zero level curves $G_1(t) = \{\mathbf{x}(t) : \phi_1(\mathbf{x},t) = 0\}$ and $G_2(t) = \{\mathbf{x}(t) : \phi_2(\mathbf{x},t) = 0\}$ coincide analytically but may differ numerically, as a result of approximate numerical procedures.

When three (or more) fluid components are involved, partitioning the domain is more complex, since "not material 1" does not necessarily imply "material 2". It is also possible for three (or more) materials to meet at a single point, a structure often referred to as a triple junction (see Figure 1).

The traditional method for representing materials has been to associate each level set function with a particular material, in the spirit of (3). Inconsistencies in material representation may develop from this model. Although algorithms exist to resolve ambiguities in material identification, they often involve ad-hoc procedures and arbitrary choices. In this paper, we describe a new level set model for multimaterial fluid dynamics which identifies each function with the two materials that it separates, in the spirit of (4). This model is not free of potential inconsistencies, but the regions where such inconsistencies may arise drop in dimension when compared to the traditional model: from a curve to a point in 2D, and from a surface to a curve in 3D. Moreover, the new method is computationally robust. This is a desirable property to have in multimaterial flow calculations considering material interfaces are physically unstable; errors near material fronts may seed instabilities and induce false interfacial dynamics over time.

Much of the literature on level set models for multimaterial fluid flow has been concerned with incompressible flow [9, 10, 14]. In incompressible flow, conservation of individual species mass translates into conservation of volume, and an important measure of computational accuracy is the ability of the zero level curve to conserve the volumes it encloses. The present work is concerned with compressible flow. Here, material designation is coupled back into the flow field via the material equation of state (EOS), which

determines the fluid pressure. The interfaces are therefore not merely carried passively by the fluid flow; they also influence its evolution.

In the following sections, we will discuss the two level set models for representing M fluid components. In Section 2, we outline the traditional level set model. We describe errors in its material representation model due to numerical diffusion and discuss existing methods for addressing these errors. In Section 3, we introduce the new model as a natural extension of the two-material model (4) to M-material flow. We detail its material representation model, provide examples illustrating its effectiveness, and demonstrate its robustness to numerical diffusion effects. In Section 4, we compare the two models using a variety of numerical tests.

2 Material Level Set Model

In order to represent M fluid components (here $M \geq 3$), multiple level set functions are required. In [4, 8, 12, 18], each of the M materials is assigned its own level set function ϕ_k, $k = 1, \ldots, M$. We refer to this as the *Material Level Set model* or MLS model for short.

The sign of $\phi_k(\mathbf{x}, t)$ defines the representation model for material k:

$$\phi_k(\mathbf{x}, t) \begin{cases} > 0 & , \text{ Material } k \\ < 0 & , \text{ Not Material } k \\ = 0 & , \text{ Boundary of Material } k \end{cases} \tag{5}$$

The zero curve $G_k(t) = \{\mathbf{x}(t) : \phi_k(\mathbf{x}, t) = 0\}$ defines the interface enclosing material k at time t. Using (5), it follows that material l is represented uniquely by the state

$$\begin{cases} \phi_k > 0 & , \quad k = l \\ \phi_k < 0 & , \quad k \neq l \end{cases} \tag{6}$$

The Y-junction in Figure 1 is represented uniquely by the signs of level curves ϕ_1, ϕ_2, and ϕ_3. It is customary to initialize each of the ϕ_k as a signed distance function to the corresponding material interface:

$$\phi_k(\mathbf{x}, 0) = \begin{cases} d(\mathbf{x}, G_k(0)) & , \quad \mathbf{x} \text{ in material } k \\ -d(\mathbf{x}, G_k(0)) & , \quad \mathbf{x} \text{ outside material } k \end{cases} \tag{7}$$

where $d(\mathbf{x}, G)$ is the minimal distance between point $\mathbf{x}$ and curve G. This is illustrated in Figure 2. Interface motion is governed by the fluid advection equation (2) for each level set function ϕ_k. At any later time $t > 0$, the respective zero level curves of the functions ϕ_k define the boundaries of the corresponding materials.

2.1 Indeterminate States

At the analytic level, this model produces a consistent picture. The material boundary segments all propagate by the same underlying velocity field, and boundary segments that coincided at $t = 0$ will also coincide at later times $t > 0$. A domain that is initially partitioned in a consistent way, will continue to be partitioned in a consistent way, with each subregion occupied by exactly one material.

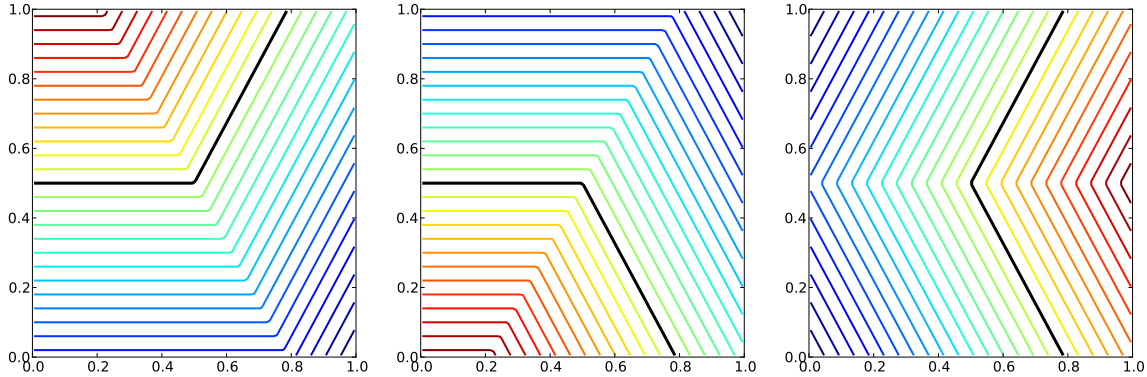

Figure 2: Representing the Y-shaped triple junction using material level set functions.

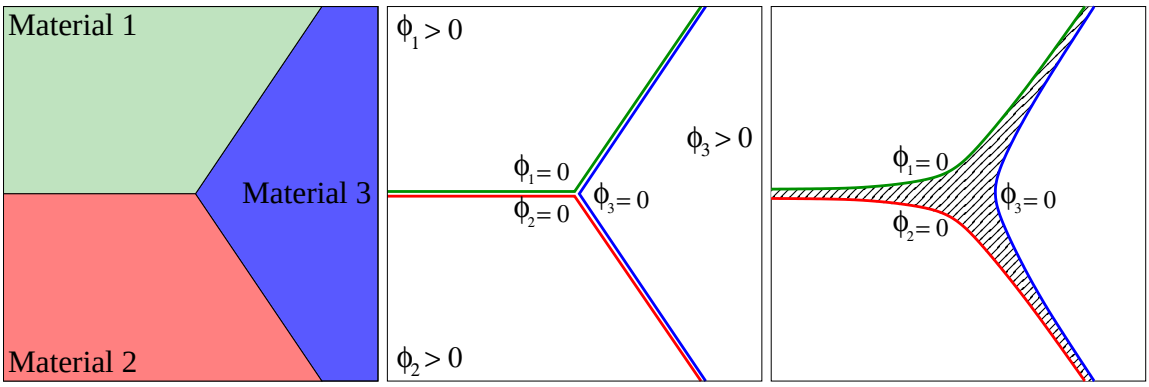

Figure 3: Y-junction schematic (left), zero curves of MLS functions (center), numerical diffusion creates an indeterminate vacuum state (right).

Numerically, however, this may not be the case. Approximate numerical procedures introduce numerical diffusion that tends to round off sharp corners in the level set functions, for example near triple junctions. The cumulative effect of numerical diffusion can generate indeterminate states in which multiple functions are positive (numerical overlap) or no functions are positive (numerical vacuum, see Figure 3).

Coupling the evolution of the individual level-set functions may successfully remove indeterminate states in MLS models, but the proposed algorithms all seem to involve arbitrary choices in the process:

For example, in [8], material designation is determined not by the collective signs of the level set functions, but rather by the level-set function that is largest in value. Repeated employment of this algorithm may lead to errors over time. In [4, 12], M-1 level-set functions are used to represent M materials. In the case of three materials, if a region is "not material 1" and "not material 2," it is necessarily "material 3." However, as illustrated in Figure 4, the reduced model is not unique, and choosing between candidate models introduces arbitrariness into material identification. In [18], a variational formulation is employed, using an additional nonlinear constraint to couple the evolution of the functions and prevents numerical overlaps and vacuums from forming. Enforcement of the constraint may give rise to spurious interface motion. In addition, the method is

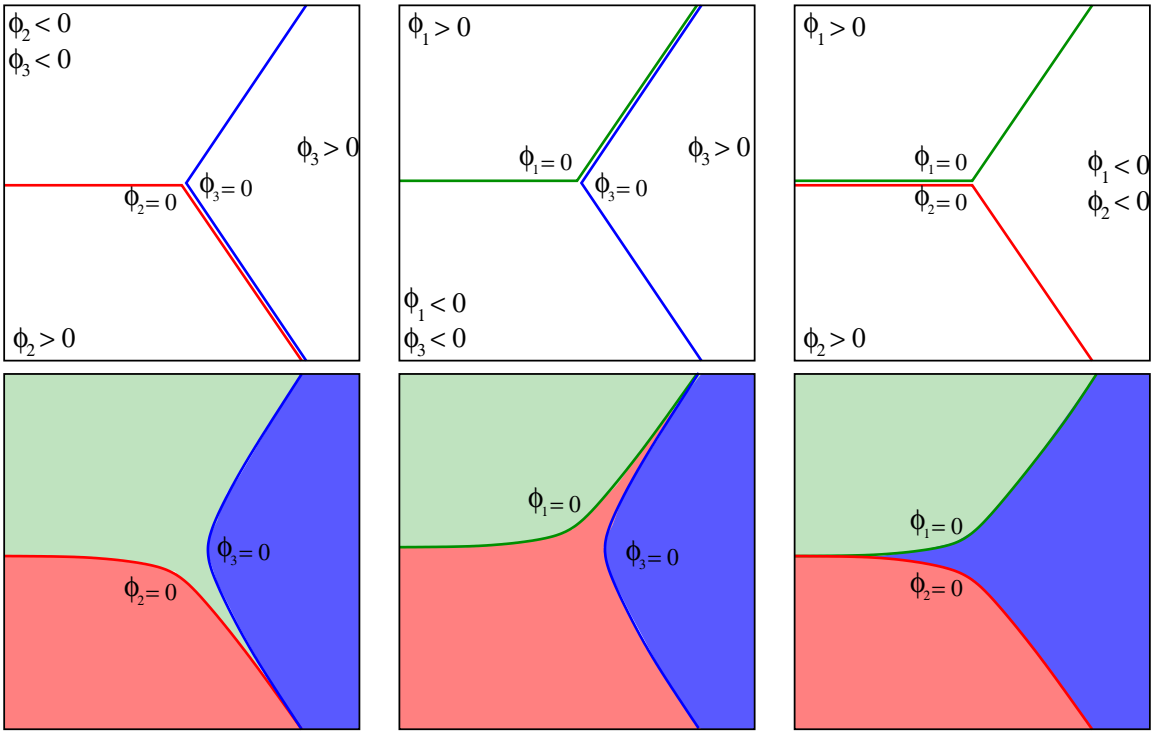

Figure 4: Representing a triple junction using two functions: initial representation (top), material locations after functions diffuse numerically (bottom).

limited to situations where a variational framework is valid.

2.2 Reinitialization

Interfaces often evolve and develop complex structures. Level set functions that start off smooth, say as distance functions, lose their smoothness over time and with it the accuracy and reliability of their predictions. A common practice is to restore smoothness near the interface by reinitialization, often resulting in improved performance [15].

In [13], the authors restore the level set function to a distance function by iterating the equation

$$\frac{\partial \phi}{\partial \tau} = \text{sign}\,(\phi_0)\,(1 - |\nabla \phi|) + \lambda H'(\phi)|\nabla \phi| \tag{8}$$

to steady state in pseudo-time τ, where H is the Heaviside function, ϕ_0 corresponds to the initial function $\phi(\tau = 0)$, and λ is a function of ϕ and ϕ_0 chosen to preserve the location of the zero level curve to within grid resolution. This redistancing algorithm, originally devised for problems involving a single level set function, preserves the sign of the function but modifies its values to restore smoothness near the interface.

The reinitialization algorithm proposed by Merriman, Bence, and Osher (MBO) in [8] applies to multiple MLS functions. The signs of the functions are first modified to eliminate indeterminate states:

$$\tilde{\phi}_k = \Big(\phi_k - \max_{m \neq k} \phi_m\Big). \tag{9}$$

Their values are then modified through a redistancing step to return smoothness to the function. This can be done, for instance, by iterating (8) for each function ϕ_k, with ϕ_0

replaced by the sign-modified function $\tilde{\phi}_k$ at $\tau = 0$. We refer to this algorithm as *MBO reinitialization*. We have implemented both the MBO algorithm and a second-order-accurate version of [13] for this paper.

Motivation for a New Model

The formation of indeterminate states points to an inherent deficiency in the MLS model: if level set functions are associated with materials, then each interface must be represented by two separate functions. When the zero curves agree to within mesh resolution, no ambiguities arise and the interface is well-represented. However, when they disagree, numerical vacuum and overlap states form. Errors often associated with numerical diffusion, such as rounding off of corners at material triple junctions, tend to exacerbate this deficiency.

In the following sections, we introduce a new model for level sets which identifies each level set function with the pair of materials it separates. The *Interface Level Set* model, or ILS model for short, generalizes the simple two-material, single-function model (4) for situations involving M materials.

3 Interface Level Sets

We define level set functions through material pairs. Let $\phi_{m,n}$ be the function corresponding to materials m and n such that

$$(\mathbf{x}, t) \quad \begin{cases} \text{in material m} & \Longrightarrow \quad \phi_{m,n}(\mathbf{x}, t) > 0 \\ \text{in material n} & \Longrightarrow \quad \phi_{m,n}(\mathbf{x}, t) < 0 \\ \text{along } (m, n) \text{ interface} & \Longrightarrow \quad \phi_{m,n}(\mathbf{x}, t) = 0 \end{cases} \tag{10}$$

If $(\mathbf{x}, t)$ is not in a region occupied by either material m or material n, the sign of $\phi_{m,n}(\mathbf{x}, t)$ is not constrained and may take on an arbitrary value. Clearly, $\phi_{m,n}(\mathbf{x}, t) > 0$ does not necessarily imply that $(\mathbf{x}, t)$ is occupied by material m, only that it *may be* occupied by material m; all we know for sure is that *it is not* occupied by material n.

Similarly, the zero curve $G_{m,n}(t) = \{\mathbf{x}(t) : \phi_{m,n}(\mathbf{x}, t) = 0\}$ is used to identify the location of the (m,n)-interface at time t. $G_{m,n}(t)$ may also contain portions that are not part of the interface. To decide which material actually occupies $(\mathbf{x}, t)$, all level set function are interrogated and a pairwise voting system is used:

$$\phi_{m,n}(\mathbf{x}, t) \begin{cases} > 0 & \Longrightarrow \quad \text{Material } m \text{ gets a vote} \\ < 0 & \Longrightarrow \quad \text{Material } n \text{ gets a vote} \end{cases} . \tag{11}$$

Under (11), no material can receive more than $M-1$ votes, and no two materials can simultaneously receive $M-1$ votes. Therefore, the material which occupies $(\mathbf{x}, t)$ receives exactly $M-1$ votes. In general, the representation of M materials using ILS functions is not unique. Whenever possible, $G_{m,n}(0)$ is extended in a smooth way into regions where it is unconstrained. Time evolution of each function $\phi_{m,n}$ again satisfies the fluid advection equation (2). We illustrate this process by example:

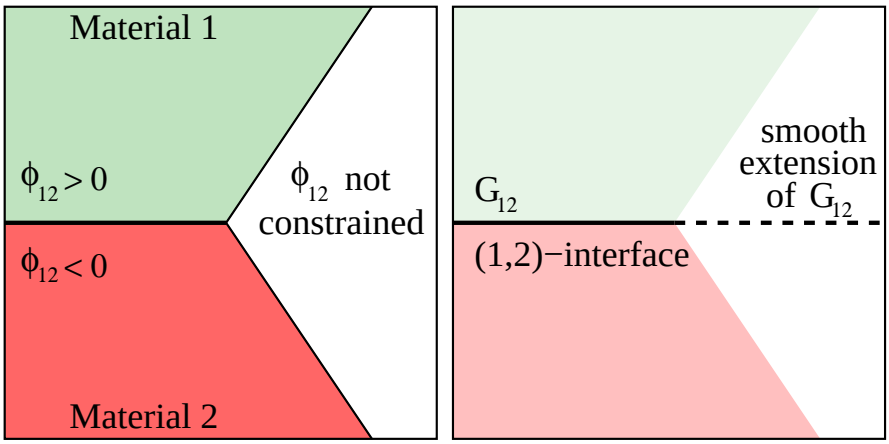

Figure 5: Defining an interface level set function: sign constraints based on material (left) and smooth extension of its zero curve into unconstrained regions (right).

3.1 Example 1: A Simple Y-Junction

The ILS model can represent the Y-junction configuration in Figure 1 using three smooth functions. To begin, let us consider materials 1 and 2. $\phi_{1,2}$ is defined to satisfy (10) but is unconstrained in the material-3 region (see Figure 5). The zero curve $G_{1,2}$ is extended into this region so that it is smooth. Values are then assigned to $\phi_{1,2}$ to initialize it as a distance function:

$$\phi_{1,2}(\mathbf{x}, 0) = \begin{cases} d(\mathbf{x}, G_{1,2}) & , \quad \mathbf{x} \text{ on the material-1 side of } G_{1,2} \\ -d(\mathbf{x}, G_{1,2}) & , \quad \mathbf{x} \text{ on the material-2 side of } G_{1,2} \end{cases} . \tag{12}$$

Repeating the process for $\phi_{1,3}$ and $\phi_{2,3}$, we obtain the functions in Figure 6. The solid lines indicate material interfaces, while the dashed lines indicate the smooth extensions of the various zero curves.

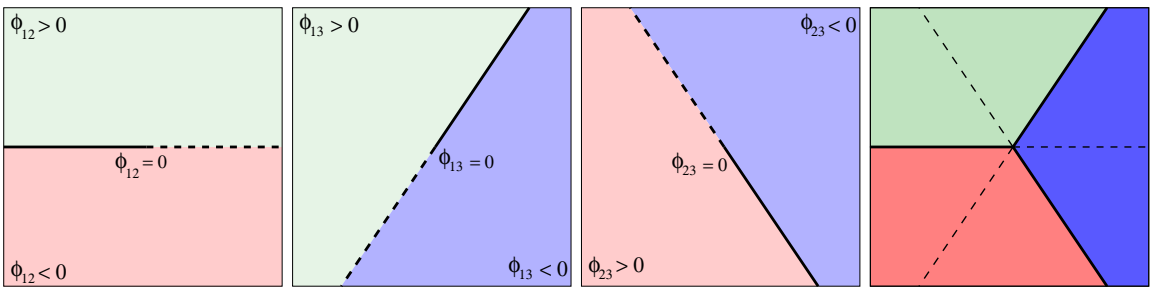

Figure 6: Schematic representation of the Y-junction using ILS functions. Solid lines are material interfaces, dashed lines are smooth extensions of zero curves.

3.2 Indeterminate States: MLS Versus ILS

We consider the occurrence of indeterminate states in the MLS and ILS models in the context of the three-material triple junction (see Figure 7).

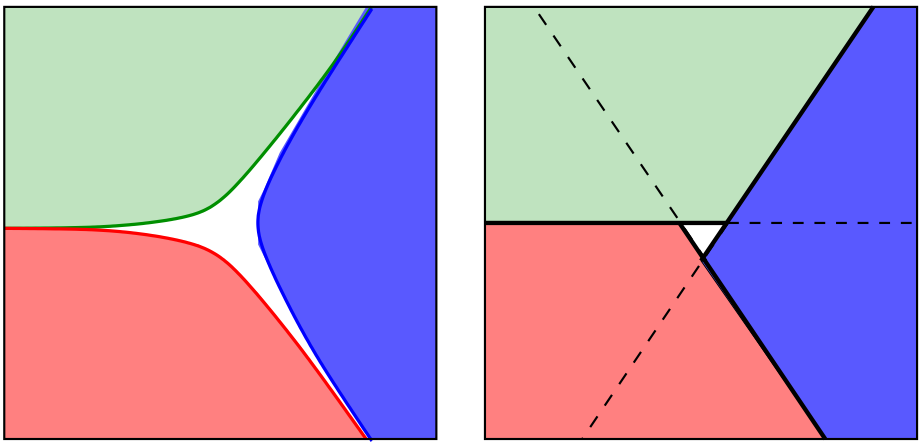

Figure 7: Comparing indeterminate states for the MLS model (left) and ILS model (right) at a triple junction. Two MLS functions fail to represent a shared interface. Three ILS functions fail to represent the same triple junction point.

The MLS model represents the Y-junction configuration in Figure 1 using three non-smooth functions. Each boundary segment is represented by zero level-curves of two different functions. If they fail to agree, for instance due to numerical diffusion rounding off sharp interface corners, then regions may arise which appear not to be occupied by any material. This is illustrated by the white region in the left schematic of Figure 7. These regions occur *along material interfaces* (and oftentimes near triple points), they are curves in two-dimensional problems, and surfaces in three-dimensional problems.

By contrast, in the ILS model, disagreements as to which material occupies a region occur when three zero curves that are supposed to intersect at a triple point "miss" each other. This is illustrated in the right schematic in Figure 7. For these regions, the voting model returns a tie, with each material receiving one vote. They occur *at the triple point itself* in two-dimensional problems, and along curves in three-dimensional problems.

In either the two- or three-dimensional case, the indeterminate regions are one dimension lower in the ILS model than in MLS. Furthermore, initializing level set functions in a smooth way near triple points renders the computation more robust to the adverse effects of numerical diffusion. While in theory, indeterminate regions may arise in the ILS model, it has been our experience that this is difficult to observe in practice (see Section 4).

3.3 Example 2: Representing a 5-Material Shock Tube

The ILS model and its pairwise voting system offers a flexible tool for representing complex configurations of materials. We further illustrate the flexibility of the model using a shock tube problem composed of five materials. This problem is motivated by experiments and simulations in [3, 11, 16]. Figure 8 gives the configuration of the materials and (one possible) initialization using 10 ILS functions.

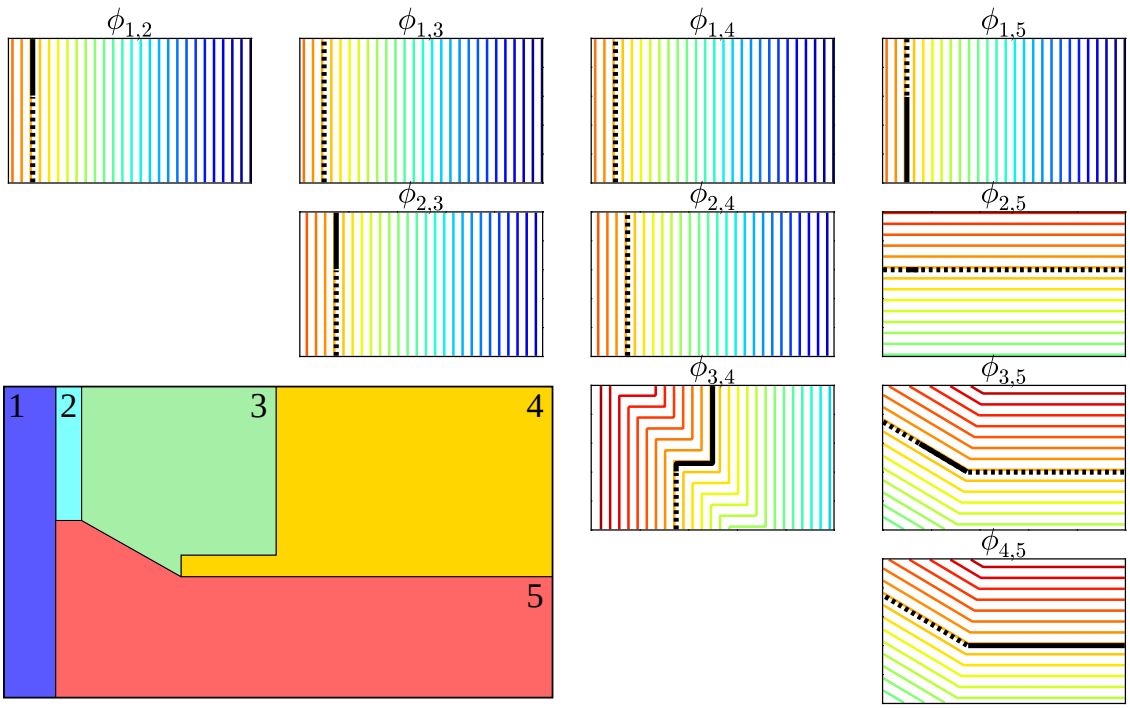

Figure 8: Representing a 5-material shock tube using 10 ILS functions. Solid lines are interfaces, dashed lines are smooth (when possible) extensions.

We use this example to illustrate the following points

(i) A general configuration of M materials may be represented by $M(M-1)/2$ ILS functions

(ii) It may be that not every pair of materials share an interface. For example, material 1 neighbors materials 2 and 5 but not 3 and 4. When the connectivity of the interfaces remains the same over time (i.e., no merging of triple junctions or topological changes in the interfaces), materials that do not share an interface initially, will not do so for $t > 0$.

In this situation it is possible to represent the material configuration by fewer than $M(M-1)/2$ level-set functions. For example, since the (1,3)-interface does not exist initially, the voting power of $\phi_{1,3}$ using (11) is simply "Material 1" if positive and "Not Material 1" if negative. This logic extends in a similar way to $\phi_{1,2}$, $\phi_{1,3}$, $\phi_{1,4}$, and $\phi_{1,5}$. The same is true for the functions $\phi_{2,3}$ and $\phi_{2,4}$ and for the functions $\phi_{3,5}$ and $\phi_{4,5}$.

For this example, five functions are sufficient to maintain the representation model. To account for fewer functions, an amended voting system may be defined, giving some functions more voting power than others. The idea is summarized in Table 1.

(iii) It is not always possible to initialize an ILS function in a smooth way. For example, the zero curve $G_{3,4}$ is non-smooth, because the (3,4)-interface contains sharp corners.

Function	Sign	Votes for Material				
		1	2	3	4	5
ϕ_1	$+$	4				
$(= \phi_{1,2} = \phi_{1,3} = \phi_{1,4} = \phi_{1,5})$	$-$		1	1	1	1
ϕ_2	$+$		2			
$(= \phi_{2,3} = \phi_{2,4})$	$-$			1	1	
$\phi_{2,5}$	$+$		1			
	$-$					1
$\phi_{3,4}$	$+$			1		
	$-$				1	
ϕ_5	$+$			1	1	
$(= \phi_{3,5} = \phi_{4,5})$	$-$					2

Table 1: Voting system for 5 ILS functions to represent the 5-material shock tube problem.

4 Numerical Tests

In the following examples, we employ a finite volume discretization. The examples involving the Euler equations are solved using a second-order upwind scheme with double minmod flux limiter [17] and dimension-by-dimension splitting. We note that problems involving material interfaces are physically unstable and tend to develop find scale structure on the scale of the grid. In the absence of (fixed) viscosity, a finer grid produces finer structure, making visual comparisons between different methodologies challenging. For this reason, the numerical results are presented on relatively coarse grids. We note, however, that differences we point out persist on finer grids.

For all numerical results, the term "redistancing" refers to applying a second-order-accurate Sussman-Fatemi scheme [13] by iterating (8) once at the end of each time step. For examples involving MLS functions, we also employ the MBO reinitialization algorithm [8]. Both algorithms are discussed in Section 2.2.

Test 1: Passive Advection of a Multimaterial Configuration

We consider a four-material test problem inspired by [8] (see Figure 9). Interfaces advect according to a prescribed flow velocity $\mathbf{u} = (3/5, 2/5)$, with periodic domain boundaries. The analytic solution at the final time $t = 5$ is equal to the initial configuration, with materials having traversed the domain three times in the x-direction and two times in the y-direction.

Figure 10 shows the initial level curves for the MLS and ILS models using a grid of 50×50 cells. Sharp corners in the MLS level curves are unavoidable and give rise to regions susceptible to numerical diffusion effects. By contrast, the ILS functions are initialized so that they are smooth everywhere. Note that although six ILS functions are used to represent four materials, only four of the functions are distinct.

We note that, due to the periodic boundary conditions, the three ILS functions composed of straight lines are in fact discontinuous across the domain boundary. It is not difficult to initialize them so that they are smooth; however, since the discontinuous por-

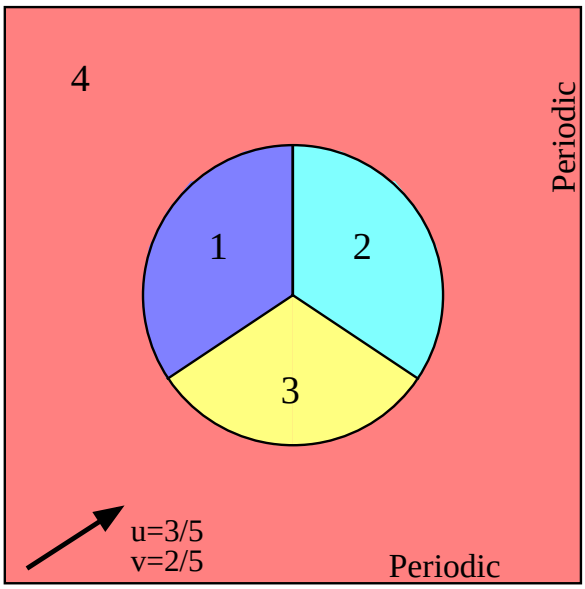

Figure 9: Initial setup for Numerical Test 1.

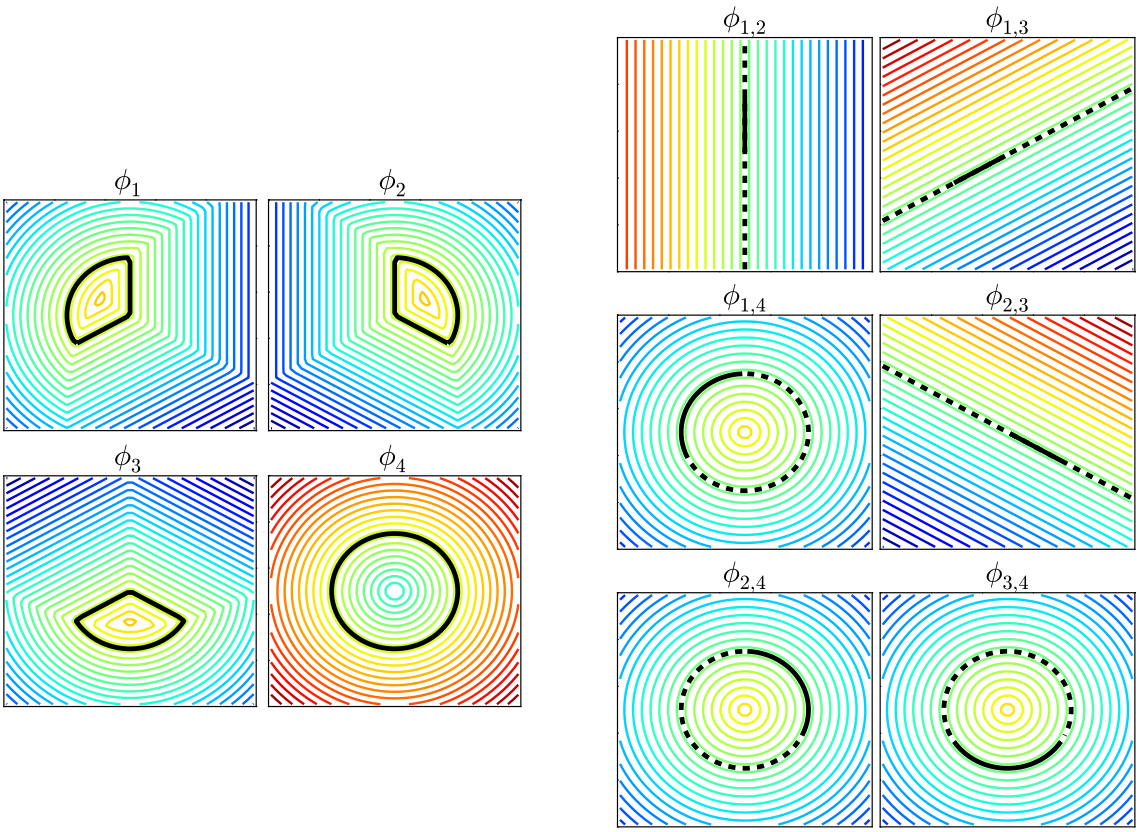

Figure 10: Initial level set functions for MLS (left) and ILS (right) models. Solid lines are interfaces, dashed lines are smooth extensions.

tions of the zero curves do not represent actual material interfaces, they do not seem to have an effect on the computed solution.

Figure 11 compares the zero level curves (black lines) to the analytic interface po-

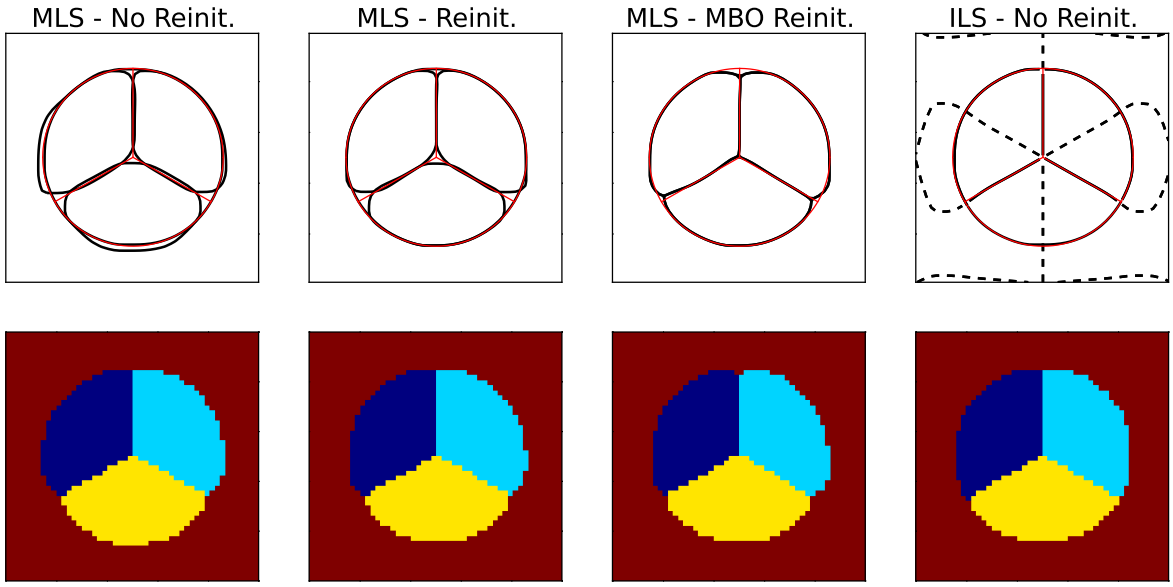

Figure 11: Comparison of zero level curve to analytic interfaces (top), color map of material locations (bottom). Models from left to right: MLS (no reinitialization), MLS (redistancing), MLS (MBO reinitialization), ILS (no reinitialization).

sitions (red lines). The ILS model is compared to three different MLS setups: (i) no reinitialization, (ii) redistancing using (8), and (iii) MBO reinitialization using (9). Color maps of material designations are provided. Whenever indeterminate states arise in the MLS model, they are resolved using the function that is largest in value.

In this example, the ILS model does not give rise to any indeterminate states, while the MLS model produces both vacuum and overlap states. This highlights the benefit of initializing level set functions in a smooth way. MBO reinitialization removes indeterminate states but leaves behind errors in interface position near triple junctions. This can be viewed as errors in volume conservation: numerical diffusion at triple junctions along the material-4 boundary cause materials 1, 2, and 3 to lose volume to material 4 (see Figure 12).

With the ILS model, interface locations and triple junction positions are in excellent agreement with the exact locations. The periodic boundary effect on the level-set functions $\phi_{1,2}, \phi_{1,3}$ and $\phi_{2,3}$ is of cosmetic significance and do not produce errors in material identification.

Material volume conservation is shown in Figure 12. The largest errors in the ILS model correspond to interactions with the periodic boundaries. Errors are significantly smaller compared to the MLS model, including computations involving reinitialization. Moreover, errors appear not to accumulate in time.

Test 2: 2D Riemann Problems on a Y-Junction

The next example involves compressible multi-material flows. The governing equations are the Euler equations

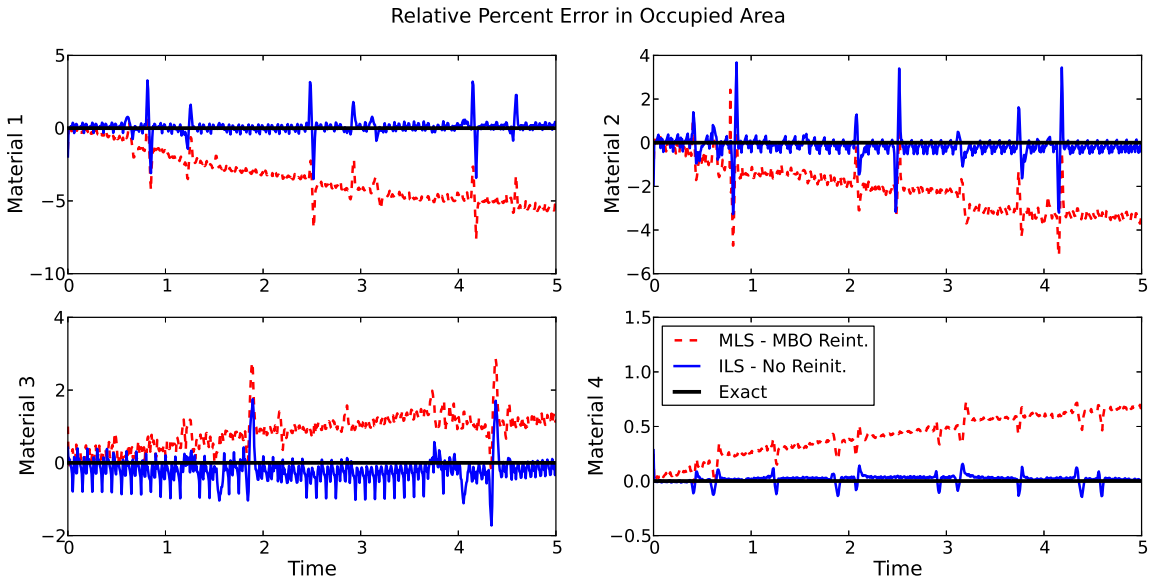

Figure 12: Relative percent error in area occupied by each material over time. Compares MLS model with MBO reinitialization (red) and ILS model with no reinitialization (blue).

$$\begin{bmatrix} \rho \\ \rho\mathbf{u} \\ E \end{bmatrix} + \nabla \cdot \begin{bmatrix} \rho\mathbf{u} \\ \rho\mathbf{u} \otimes \mathbf{u} + p\mathbb{I} \\ \mathbf{u}(E+p) \end{bmatrix} = 0 \tag{13}$$

with ideal gas equation of state (EOS)

$$p = (\gamma - 1)\left(E - \frac{1}{2}\rho u^2\right). \tag{14}$$

Here ρ gives the fluid density, E the total energy, and p the pressure. The adiabatic index γ is a material-dependent quantity and is correlated with the compressibility of a fluid component.

It is well known that naive numerical discretizations of material-dependent terms may result in oscillations across compressible material fronts [1]. Algorithms that circumvent these oscillations are available and include [5, 6, 7]. We have adopted the single-fluid algorithm proposed in [7]. (See [2] for a comprehensive overview.)

We consider Riemann data across a Y-shaped triple junction (see Figure 13). The domain is a tube with solid walls at the top and bottom boundaries and open inflow/outflow boundary conditions on the left/right. The gas is initially at rest, with

$$(\rho, p, \gamma)_1 = (1, 1, 1.6), \qquad (\rho, p, \gamma)_2 = (1, 0.1, 1.5), \qquad (\rho, p, \gamma)_3 = (0.125, 0.1, 1.4)$$

Pressure discrepancies across the (1,2)- and (1,3)-interfaces send planar shock waves in the direction normal to each interface. The differing densities and compressibilities cause the shock to travel faster in the less-dense material. This creates shear across the (2,3)-interface, causing the interface to roll up and subsequently develop a complex interface structure.

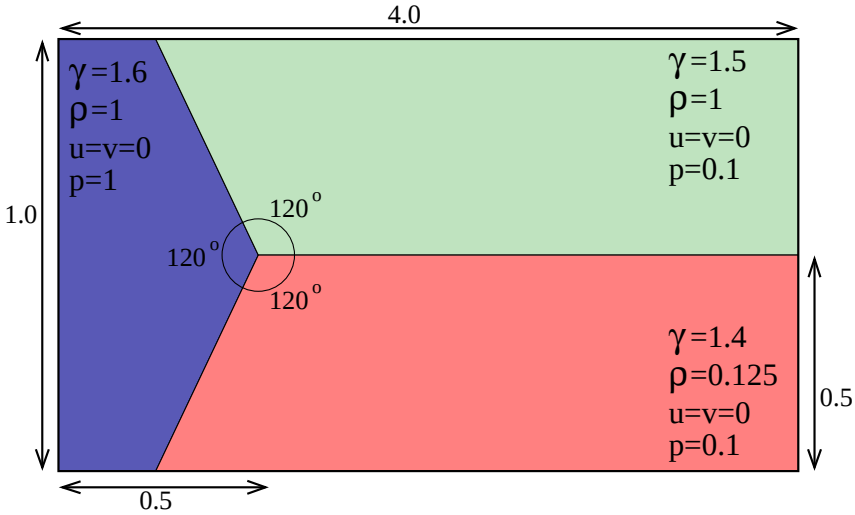

Figure 13: Initial setup for Numerical Test 2.

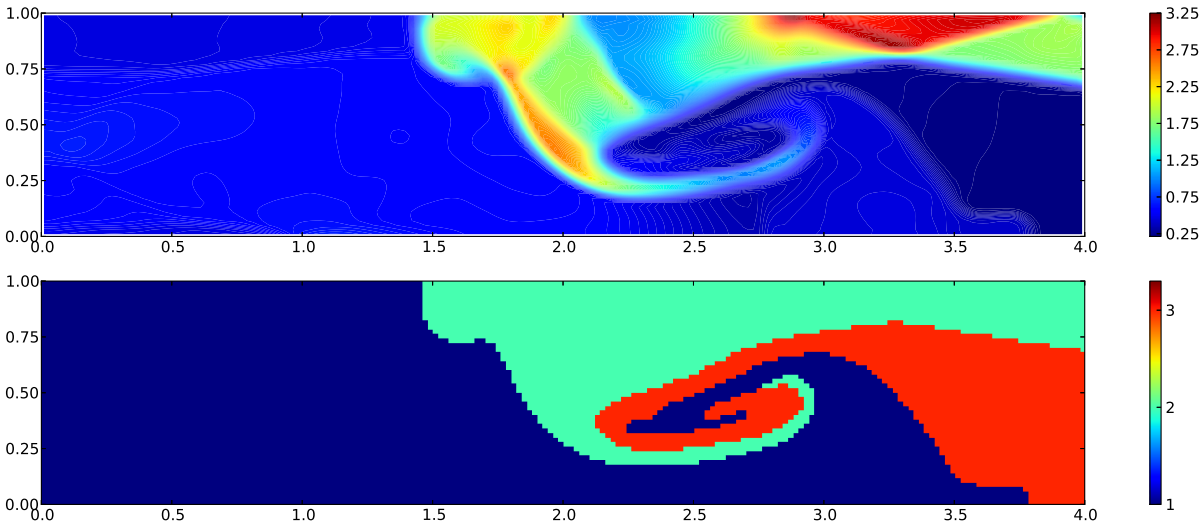

Figure 14: Density contours (top) and material locations (bottom) using the MLS model

We compare results at time $t = 3$. At this time, the shocks have exited the domain, and the interfaces near the triple point have undergone significant roll-up. Figure 14 gives density contours and material locations for the full domain. The MLS model with no reinitialization was used for this example.

Figure 15 compares the final material locations as well as each zero level curve, colored by the specific material it tracks. The top three rows compare the MLS model without reinitialization, with redistancing, and with MBO reinitialization. The bottom two rows compare the ILS model without reinitialization and with redistancing. We present results using a mesh of 200×50 cells.

We focus on the MLS model first. If no reinitialization algorithm is applied (top), a vacuum state develops, as highlighted in gray. Material designation in this region is assigned arbitrarily using the MLS function that is largest in value. Redistancing (middle) does not prevent indeterminate states; both vacuum and overlap states develop,

again highlighted in gray. We further note that repeated redistancing influences the motion of the level curves over time and alters the final location of material fronts. MBO reinitialization removes indeterminate states; however, arbitrary logic and repeated redistancing leads to discrepancies as compared with the previous MLS results.

All three MLS examples depict changes in material topology, with materials breaking off and forming "islands" inside other material subregions. This phenomenon is observed primarily within indeterminate regions, where material identification becomes arbitrary. We further observe that the material topology differs quite significantly between the three sets of results.

For the ILS zero curves, solid lines indicate material interfaces, while dashed lines indicate their (initially smooth) extensions. We observe that the ILS model is not immune to indeterminate states, as indicated by the small island of material 2 (green) inside the roll-up region, and that reinitialization does not prevent this from happening. Nonetheless, we observe that both ILS simulations, with and without redistancing, give a qualitatively consistent picture of material locations.

As a qualitative measure of solution reliability, we compare material locations derived from level set data to material interface locations derived from Lagrangian marker particles. We distribute 55,000 marker particles along the initial interfaces and advect each particle at its local flow velocity using a two-stage Runge-Kutta time integration. The marker particles are passively advected and their final location is compared to the level set results. Results are shown in Figure 16. The white-black transition region gives the material boundary as determined by the level set model; the red curve gives the material boundary as determined by the marker particles.

Both models agree with the marker particles, with differences observed primarily in the roll-up region. Here level sets are limited by grid resolution and do not capture the sub-grid filamentary structure observed in the marker particle interfaces. It is difficult to make accuracy claims for this problem, but we note that in these computations the MLS model requires reinitialization at each time level. The ILS model arrives at a consistent numerical solution without the need of reinitialization, despite the complex dynamics in the roll-up region.

Test 3: Planar Shock Through a 5-Material Shock Tube

We consider a Mach number 8 shock wave striking the five-material shock tube described in Section 3.3. Due to symmetry about the center line, the problem is solved on only the top half of the domain. Figure 17 gives the initial setup. The materials differ in density and adiabatic index, with values based on physical considerations from radiative shock tube experiments in [11, 16]. Materials correspond to beryllium (blue), gold (cyan), acrylic (green), plastic (dark yellow), and xenon gas (red). Pressure is normalized to one and velocity is zero everywhere initially, with the exception of the post-shock (dark blue) region. The left/right domain boundaries satisfy inflow/outflow boundary conditions, and the top and bottom boundaries represent solid walls.

This is a challenging test problem involving five material species of vastly different densities and compressibilities, a strong shock front, and fine-scale flow features. The shock travels faster through the low-density xenon gas than it does through the higher-density gold, acrylic, and plastic, generating shear and leading to interface roll-up. As the shock compresses the gas ahead of the beryllium, the beryllium continues to travel down the shock tube, leading to filaments of xenon gas. We use a fixed grid of 200×100

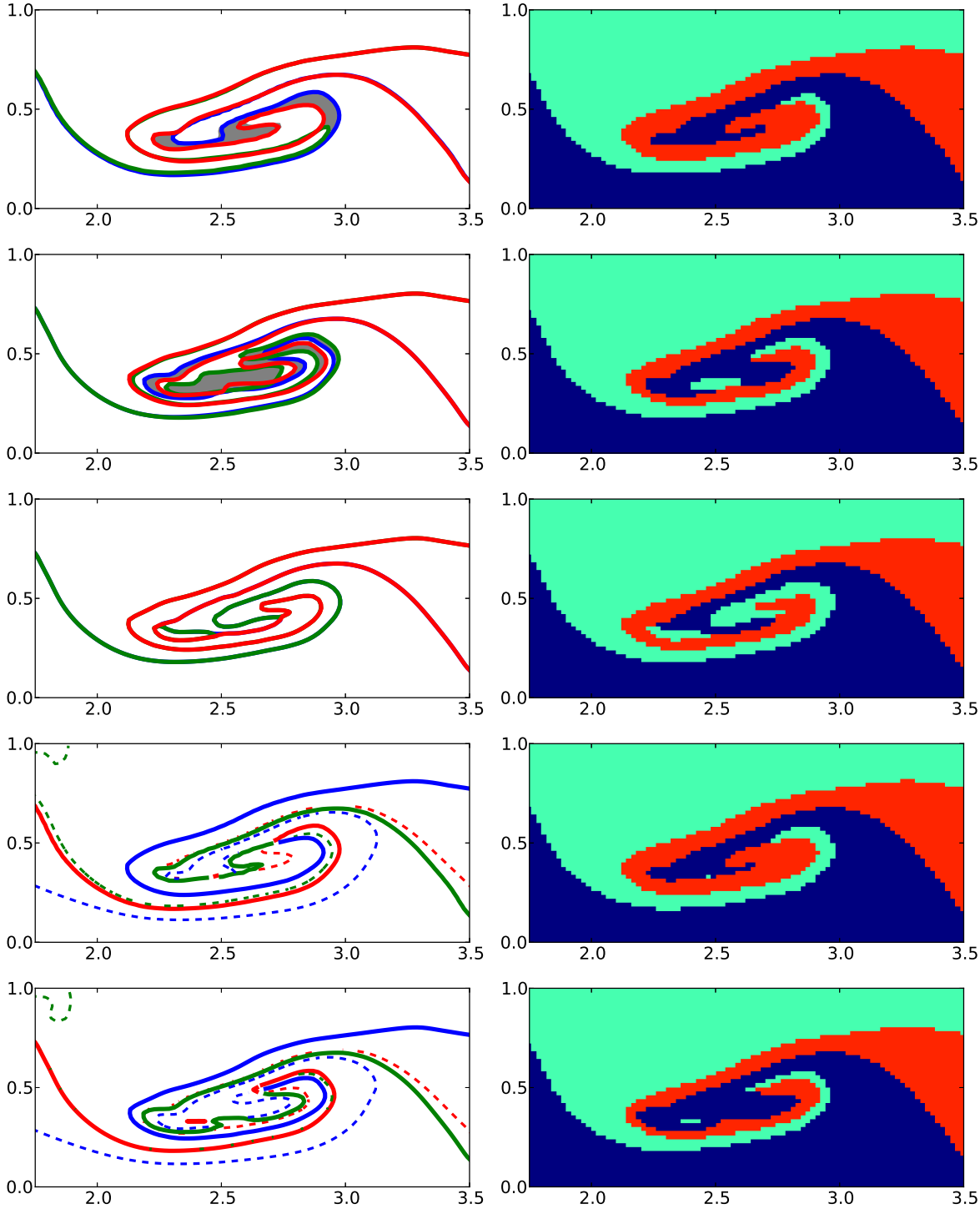

Figure 15: Zero curves (left) and material locations (right): (i) MLS without reinitialization, (ii) MLS with redistancing, (iii) MLS with MBO reinitialization, (iv) ILS without reinitialization, (v) ILS with redistancing.

cells and integrate to a final time of $t = 0.08$. We note that differences observed between models at this grid resolution persist to finer grids, but interfacial instabilities make these differences more difficult to visualize.

Results comparing MLS and ILS computations with and without reinitialization are

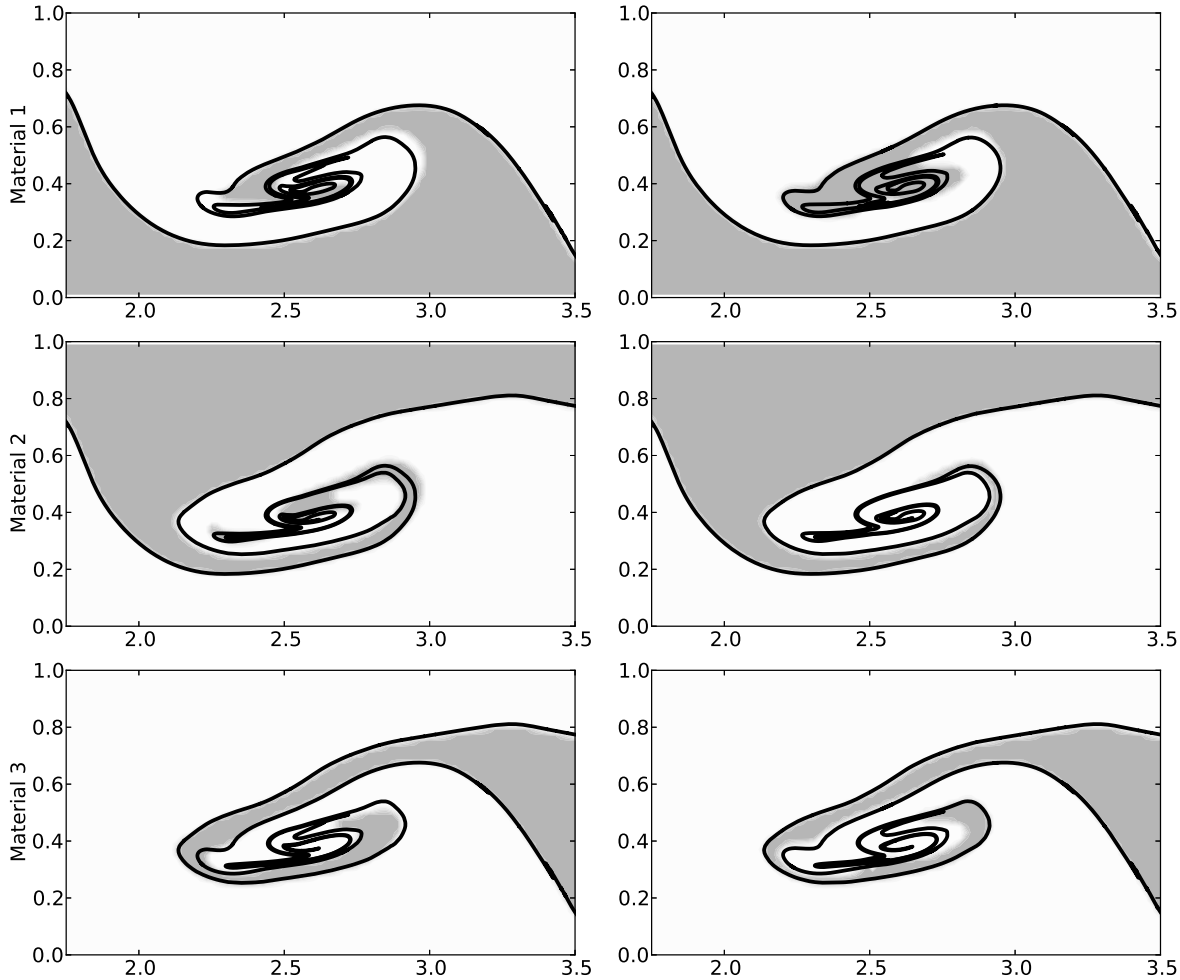

Figure 16: Material locations from level set models (gray regions) and material boundaries from Lagrangian marker particles (black lines): MLS with MBO reinitialization (left) and ILS with no reinitialization (right).

shown in Figure 18. We observe three significant features:

(i) The ILS model without reinitialization appears to best capture the fine-scale filamentary structure present in the xenon gas (red).

(ii) No indeterminate states were produced during each of the ILS simulations. By comparison, vacuum and overlap states were produced throughout the MLS simulation without reinitialization.

(iii) The MLS model with reinitialization fails to resolve gold (cyan) in this simulation. Numerical diffusion erodes the positive part of the corresponding MLS function causing the material to effectively disappear.

We compare results obtained by Lagrangian marker particles in Figures 19 and 20. 41,500 particles are distributed along the initial interfaces, for an initial particle spacing of approximately 5×10^{-5}. Both models capture interface positions consistent with the particles reasonably well, but the fine structure reveals differences:

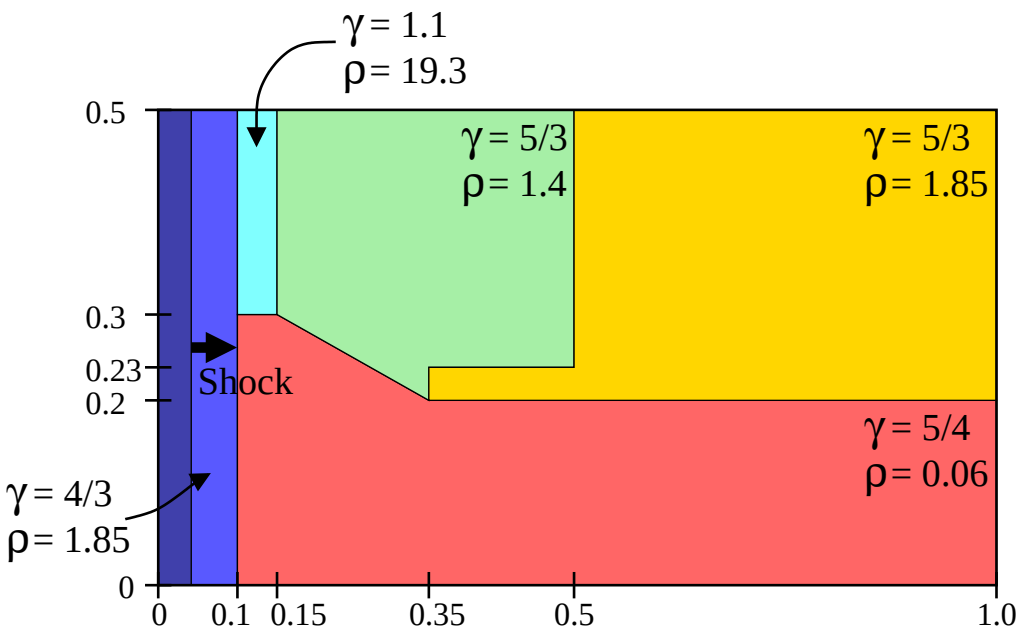

Figure 17: Initial setup for Numerical Test 3.

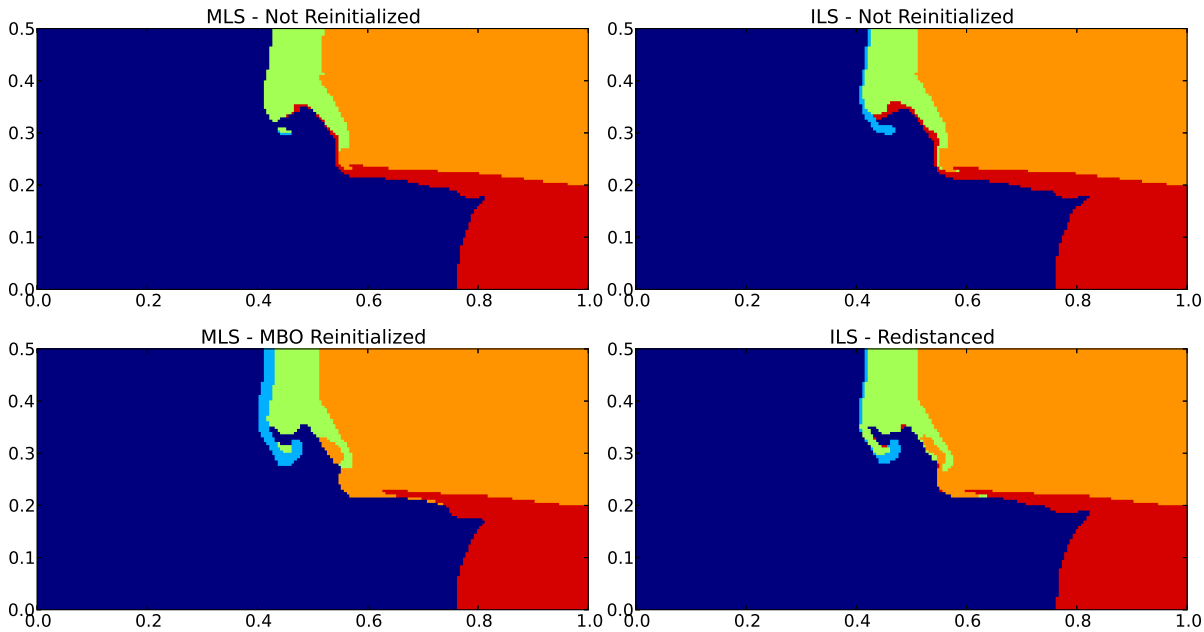

Figure 18: Final material locations for the MLS model (left) and ILS model (right) under various reinitialization methodologies.

(i) For the MLS simulation, materials 3 and 4 have developed disconnected regions. This is inconsistent with representations from both the particles and the ILS model. Running the same simulation on a finer grid creates structure at even finer scales but does not lead to global reconnection of the materials.

(ii) The material 2 boundary determined from the MLS curves is in clear disagreement with the particle locations. This is not surprising, considering the MLS model

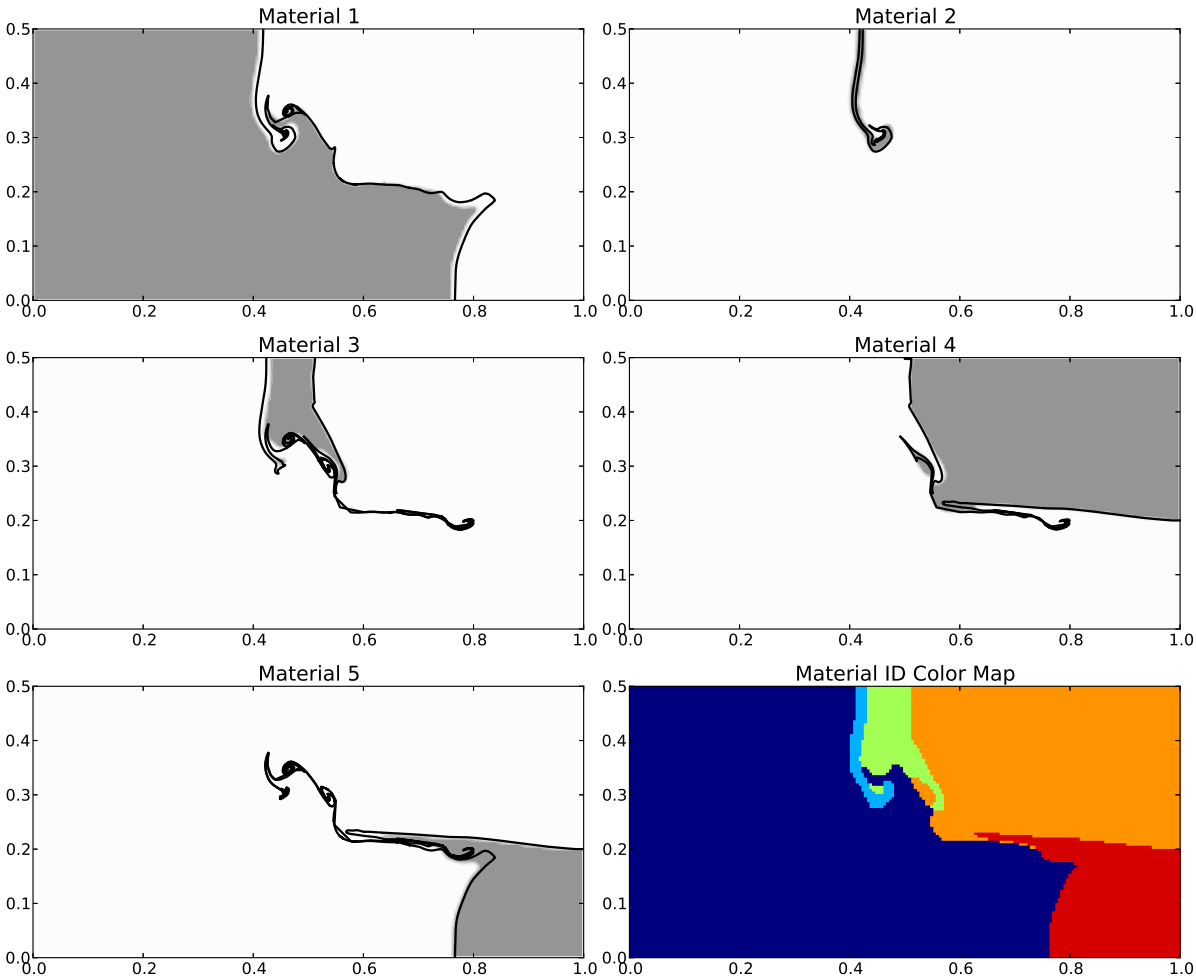

Figure 19: Material locations from the MLS model with MBO reinitialization (gray regions) and material boundaries from Lagrangian marker particles (black lines).

without MBO reinitialization is unable to represent material 2 on this grid (see Figure 18). Although MBO reinitialization corrects this error, repeated reinitialization appears to overcompensate, increasing the overall amount of material 2 in the domain.

(iii) The ILS model appears to be free of these shortcomings: It resolves fine-scale filamentary structure without producing disconnected material regions, and its material boundaries are consistent with the marker particles, even on a relatively-coarse grid. Moreover, this is accomplished without employing any reinitialization or redistancing scheme.

5 Summary

We have presented a new level set model for representing arbitrary multimaterial configurations for two-dimensional fluid flow problems. The new model identifies each level set function with the two materials it separates, rather than the standard approach that identifies each function with an individual material. The new model, while not immune

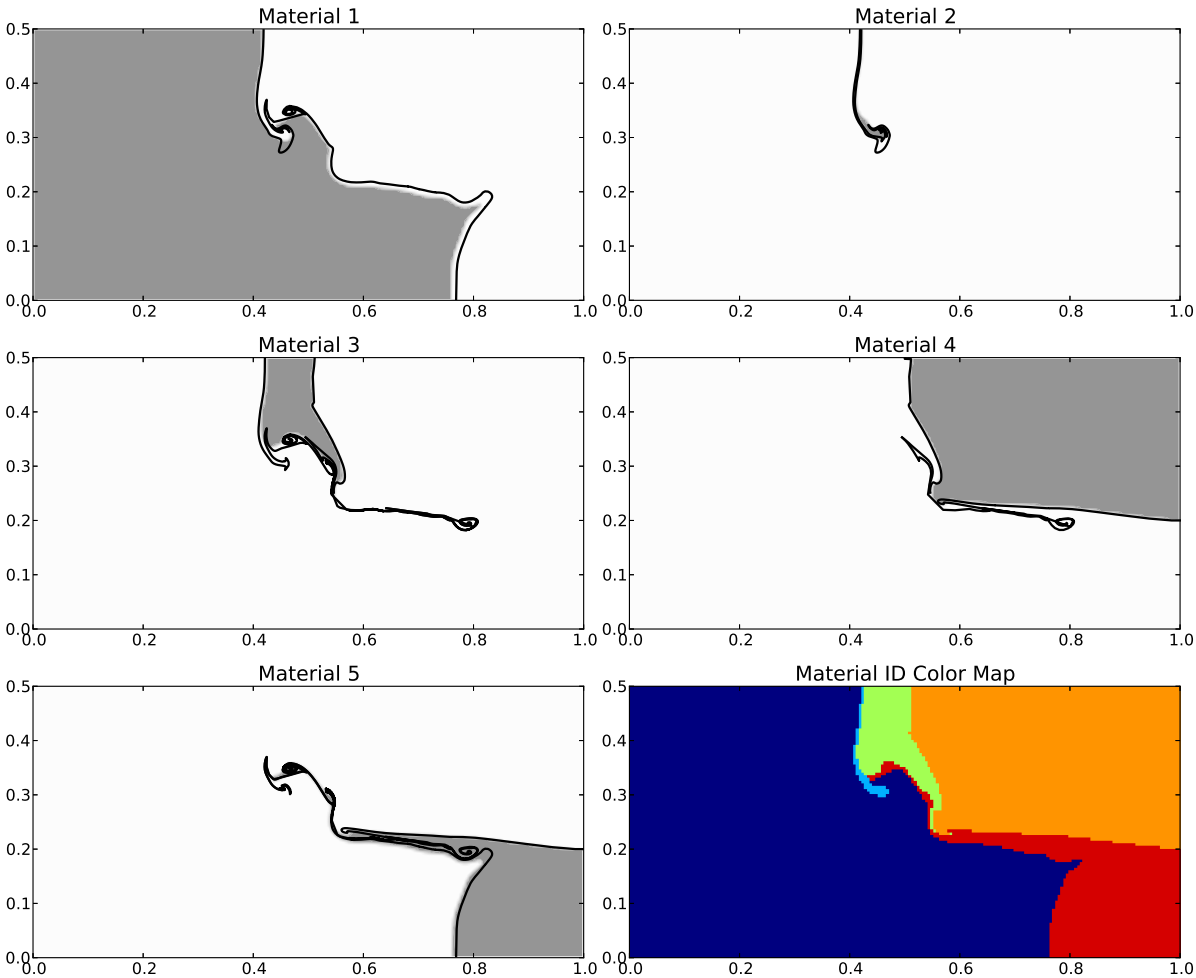

Figure 20: Material locations from the ILS model with no reinitialization (gray regions) and material boundaries from Lagrangian marker particles (black lines).

to material ambiguity, is much less likely to manifest indeterminate material states near triple junctions. Furthermore, the model avoids the need for reinitialization of the level set functions, effectively saving on computational costs and preventing degradation in solution quality brought about by excessive numerical diffusion. Finally, numerical results establish the robustness of the model as well as its ability to resolve fine scale features.

References

[1] R. Abgrall. How to prevent pressure oscillations in multicomponent flow calculations: A quasi conservative approach. J. Comput. Phys., 125(1):150 – 160, 1996.

[2] R. Abgrall and S. Karni. Computations of compressible multifluids. J. Comput. Phys., 169(2):594 – 623, 2001.

[3] R.P. Drake, E. S. Myra, M. J. Grosskopf, E. Rutter, and B. Torralva. Behavior of irradiated low-z walls and adjacent plasma. In Bulletin of the American Physical Society, volume 55 of 52nd Annual Meeting of the APS Division of Plasma Physics, 2010.

[4] S. Esedoḡlu and P. Smereka. A variational formulation for a level set representation of multiphase flow and area preserving curvature flow. Commun. Math. Sci., 6(1):125–148, 2008.

[5] R. Fedkiw, T. Aslam, B. Merriman, and S. Osher. A non-oscillatory eulerian approach to interfaces in multimaterial flows (the ghost fluid method). J. Comput. Phys., 152(2):457 – 492, 1999.

[6] S. Karni. Multicomponent flow calculations by a consistent primitive algorithm. J. Comput. Phys., 112(1):31 – 43, 1994.

[7] S. Karni and R. Abgrall. Ghost-fluids for the poor: A single fluid algorithm for multifluids. In Hyperbolic Problems: Theory, Numerics, Applications:, volume 1 of Proceedings of the 10th International Conference on Hyperbolic Problems, pages 1–10, 2001.

[8] B. Merriman, J. K. Bence, and S. J. Osher. Motion of multiple junctions: A level set approach. J. Comput. Phys., 112(2):334 – 363, 1994.

[9] R.R. Nourgaliev and T.G. Theofanous. High-fidelity interface tracking in compressible flows: Unlimited anchored adaptive level set. J. Comput. Phys., 224(2):836 – 866, 2007.

[10] E. Olsson and G. Kreiss. A conservative level set method for two phase flow. J. Comput. Phys., 210(1):225 – 246, 2005.

[11] K. G. Powell, R. P. Drake, J. P. Holloway, B. van der Holst, S. Karni, W. Martin, E. S. Myra, I. V. Sokolov, Q. Stout, and G. Toth. A 3d, parallel, solution-adaptive model for radiative shocks. In Bulletin of the American Physical Society, volume 54 of 51st Annual Meeting of the APS Division of Plasma Physics, 2009.

[12] K. Smith, F. Solis, and D. Chopp. A projection method for motion of triple junctions by level sets. Interfaces and Free Boundaries, pages 263–276, 2002.

[13] M. Sussman and E. Fatemi. An efficient, interface-preserving level set redistancing algorithm and its application to interfacial incompressible fluid flow. SIAM J. Sci. Comput., 20(4):1165–1191, February 1999.

[14] M. Sussman and E. G. Puckett. A coupled level set and volume-of-fluid method for computing 3d and axisymmetric incompressible two-phase flows. J. Comput. Phys., 162(2):301 – 337, 2000.

[15] M Sussman, P Smereka, and S Osher. A level set approach for computing solutions to incompressible two-phase flow. J. Comput. Phys., 114(1):146 – 159, 1994.

[16] B. van der Holst, G. Toth, I. V. Sokolov, K. G. Powell, J. P. Holloway, E. S. Myra, Q. Stout, M. L. Adams, J. E. Morel, S. Karni, B. Fryxell, and R. P. Drake. Crash: A block-adaptive-mesh code for radiative shock hydrodynamicsimplementation and verification. The Astrophysical Journal Supplement Series, 194(2):23, 2011.

[17] B. van Leer. Towards the ultimate conservative difference scheme iii. upstream-centered finite-difference schemes for ideal compressible flow. J. Comput. Phys., 23(3):263 – 275, 1977.

[18] H.-K. Zhao, T. Chan, B. Merriman, and S. Osher. A variational level set approach to multiphase motion. J. Comput. Phys., 127(1):179 – 195, 1996.

Prepared by LLNL under Contract DE-AC52-07NA27344